1D energy transport in a strongly scattering laboratory model

Kasper van Wijk,[1] Matthew Haney,[2] and John A. Scales[1]
[1]*Physical Acoustics Laboratory, Colorado School of Mines, Golden, Colorado 80401, USA*
[2]*Center for Wave Phenomena, Colorado School of Mines, Golden, Colorado 80401, USA*
(Received 10 January 2003; published 31 March 2004)

Radiative transfer (RT) theory is often invoked to describe energy propagation in strongly scattering media. Fitting RT to measured wave field intensities is rather different at late times, when the transport is diffusive, than at intermediate times (around one extinction mean free time), when ballistic and diffusive behavior coexist. While there are many examples of late-time RT fits, we describe ultrasonic multiple scattering measurements with RT over the entire range of times—from ballistic to diffusive. In addition to allowing us to retrieve the scattering and absorption mean free paths independently, our results also support theoretical predictions in 1D that suggest an intermediate regime of diffusive (nonlocalized) behavior.

DOI: 10.1103/PhysRevE.69.036611 PACS number(s): 42.25.Dd, 43.35.+d, 91.30.Fn, 95.30.Jx

I. INTRODUCTION

The past decades have seen such tremendous advances in understanding wave propagation in disordered media [1–3] that applications have found their way into medical imaging [4,5], seismology [6–8], and communication [9,10]. However, theoretical questions remain about wave localization [11,12] and the breakdown of diffusion, in the form of less-than-exponential decay of the intensity [13,14]. Wave propagation is localizing in infinite disordered media of dimension$\leqslant$2 [15], but two-dimensional (2D) experimental data in strongly scattering media have been explained by diffusive models (e.g., [16,17]), indicating that when the localization length is greater than the sample size, the diffusion model can be valid [3,18]. Experimental studies of truly 1D systems are rare; a recent exception may be isolated chains of atoms in a Bose gas in Ref. [19]. Even though in practice many models appear macroscopically 1D, microscopically they are of higher dimension. One example is light propagating in a thin wire. While the wire provides a 1D geometry, microscopically one can think of a wire as a collection of chains of particles. Recent studies have shown that such small deviations from 1D can prevent the interference effects of scattered waves necessary for localization. [See recent discussions on nanowires (e.g., [20–22]).]

In this paper, we study energy propagation in a strong-scattering finite medium over distances on the order of an extinction mean free path that can be described by 1D radiative transfer. In this case, the localization length must be larger than the sample size. We fit the incoherent as well as the coherent signal. This explicit fit of the entire range of observations allows an independent estimation of the scattering and absorption lengths, parameters crucial in the discussion of localization versus absorption [11,12].

A. Experiment

To achieve greater understanding of wave propagation in finite disordered media, we probe a grooved model with ultrasonic surface waves. In ultrasonics, the amplitude and phase of elastic waves provide direct measurements of coherent and incoherent signal [16,17,23,24], while surface (wave) models allow access to the scattering medium between scatters. Also, because our experiments are macroscopically 1D, scattering is limited to two directions, making even the most complicated scattering paths tractable [25].

Our model consists of an aluminum block (28 cm$\times$23 cm$\times$21.5 cm) with an aligned pattern of grooves extending over one of its faces. This pattern is quasiperiodic [45] and increases in complexity as the sequence gets longer [26,27]. The source is an angle-beam transducer, driven by one period of a 250-kHz tone burst that launches surface waves perpendicular to the grooves [28,29]. The surface waves are effectively planar over the 7-cm width of the source [30]. The grooves are nominally 1 mm wide by 3 mm deep [31], and there are 55 grooves in 15 cm. Because the dominant wavelength of the surface waves is about 12 mm, there are many scatterers per wavelength.

The wave field is detected with a scanning laser vibrometer that measures absolute particle velocity on the surface via the Doppler shift and is digitized at 14-bit precision. We terminate recording before significant energy reflected from the model boundaries reaches the detector. This setup allows us to measure multiply scattered waves between the scatterers (i.e., *inside* the scattering medium). To obtain ensemble measurements over the disordered medium, measurements at 43 fixed source-detector distances x are collected for different positions in the groove sequence.

B. Theory

Radiative transfer (RT) can be derived from energy balance considerations [2,32] and describes the ensemble-averaged intensity in strongly scattering media. Often this model is intuitively explained by a random walk of photons or phonons between scatterers in a homogeneous background material [33,34]. A general scalar radiative transfer equation in 1D is

$$\frac{\partial I_r}{\partial t}+v\frac{\partial I_r}{\partial x}=\frac{vR}{\ell_s}(I_l-I_r)-\frac{vI_r}{\ell_a}+S_r,$$

$$\frac{\partial I_l}{\partial t}-v\frac{\partial I_l}{\partial x}=\frac{vR}{\ell_s}(I_r-I_l)-\frac{vI_l}{\ell_a}+S_l. \qquad (1)$$

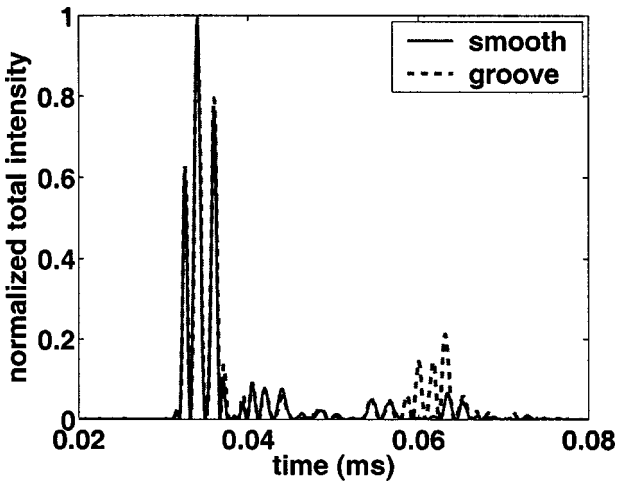

FIG. 1. Total field for a fixed x on the face of the model with a single groove. The energy backscattered from the groove arrives around 0.06 ms. For this particular measurement, the tone burst consists of two periods of a 250-kHz sine wave.

The intensity I—or average squared wave field—as a function of time t and distance x is split in left- and right-going intensity with the subscripts l and r, respectively. The characteristic absorption mean free path is ℓ_a, while v is the energy velocity and ℓ_s the scattering mean free path. S is the source term (also split) and R denotes the backscattering cross section. The separation of the field into two directions of propagation is known as two-stream theory [35,36]. In 1D, this approach is exact for RT.

The Green's function of the 1D scalar radiative transfer equation was derived long ago in elastic and isotropic media [32,37], but a more general solution including absorption and a directional source is $I=I_l+I_r$ [8]:

$$I(x,t)=\exp[-vt(R/\ell_s+1/\ell_a)]\left[\delta(x-vt)+\frac{Ru(vt-|x|)}{\ell_s}\left(I_0(\eta)+\sqrt{\frac{vt+x}{vt-x}}I_1(\eta)\right)\right]. \quad (2)$$

The argument of the modified Bessel functions of order zero (I_0) and one (I_1) is

$$\eta=(R\sqrt{(vt)^2-x^2})/\ell_s,$$

where u is the step function to assure causality in the system. Note that in 1D, the extinction mean free path (the length associated with a $1/e$ decay of the intensity) is $1/\ell_{\rm ext}=R/\ell_s+1/\ell_a$ [8,32,33]. The Dirac δ function represents the coherent signal, while the term with the modified Bessel functions describes the incoherent signal. Both decay exponentially depending on absorption and scattering (the latter being a redistribution of energy). However, the incoherent signal shows an extra scattering dependence in the argument of the Bessel functions. Furthermore, for a unidirectional source, the I_1 term represents the incoherent intensity propagating away from the source and the I_0 term is the incoherent intensity in the other direction [8].

II. ANALYSIS OF THE DATA

A. Single scattering

Wave propagation in the presence of grooves as in our model is complicated (e.g., [38]). To illustrate the scattering properties, we measure the total wave field in the presence of a single groove. Figure 1 contains the total wave field measured on the top of the face with a single groove, recorded at a point between the source and the groove, as well as in the absence of grooves. The direct arrival of the wave is present in both experiments at 0.035 ms, but a reflected signal in the presence of a groove arrives at the detector at 0.06 ms. Other phases on the smooth face of the model are due to ringing of the source. From these measurements, we estimate the backscattering cross section for a single scatterer to be $R=0.15$.

To improve our understanding of the scattering process, we move the source to the edge of the block, and scan the side (see the left panel of Fig. 2 for the setup). In an isotropic and elastic half-space, Rayleigh waves only have particle motion in the direction of propagation and in the vertical

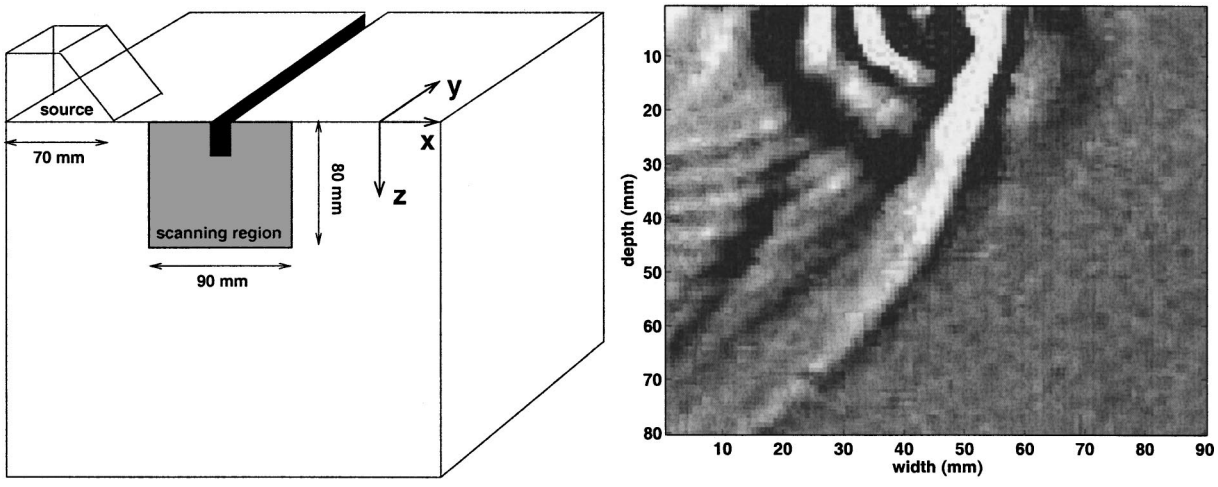

FIG. 2. Left: experimental configuration, where the source is perpendicular to a single groove on the top of the block while the detector scans the side. Right: snapshot of particle motion in the scanned region after the incident field scattered off a single groove. Note that the groove is 1 mm wide and 2.75 mm deep, a fraction of the dominant wavelength.

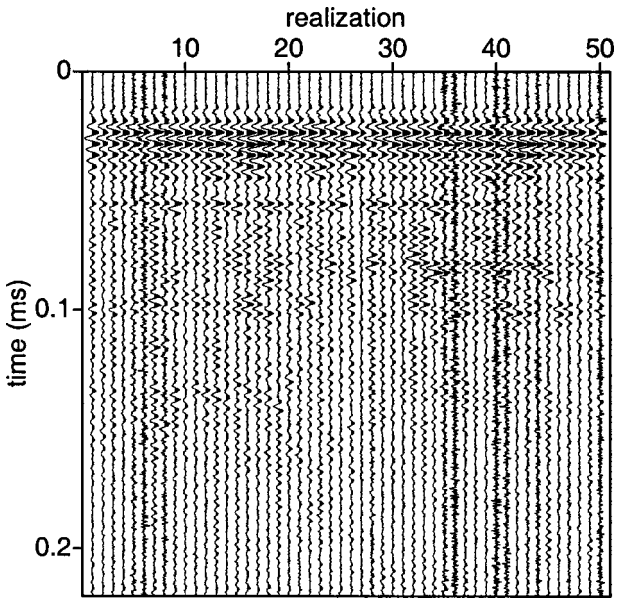

FIG. 3. Wave fields for 50 realizations at $x=4$ cm for different source-detector positions in the groove sequence. Noisier wave fields (for instance, realization 40) are due to a reduction in surface reflectivity, degrading the optical measurement.

plane. However, placing the source on the edge of an aluminum block breaks the symmetry and excites out-of-plane particle motion. This component is measured on the side in an area surrounding a single groove. Reference [39] contains a full movie of the measured scattering process. A snapshot of the wave field (i.e., an image of the wave field at a single point in time) shortly after the incident Rayleigh wave interacts with the groove is shown in the right panel. The almost linear and bright event is the transmitted field, while the other bright event is the reflected Rayleigh wave. On the left side of the right panel, weak body waves are excited by the source. The semicircles centered around the groove are body waves diffracted as the Rayleigh wave encounters the groove. This body-wave energy is lost from the surface-wave energy. These body waves return to the surface, after reflecting off the bottom of the block, but do not reenter the surface model in the time of recording. This is why the body-wave diffractions are treated as an absorptive loss term in our 1D surface-wave model.

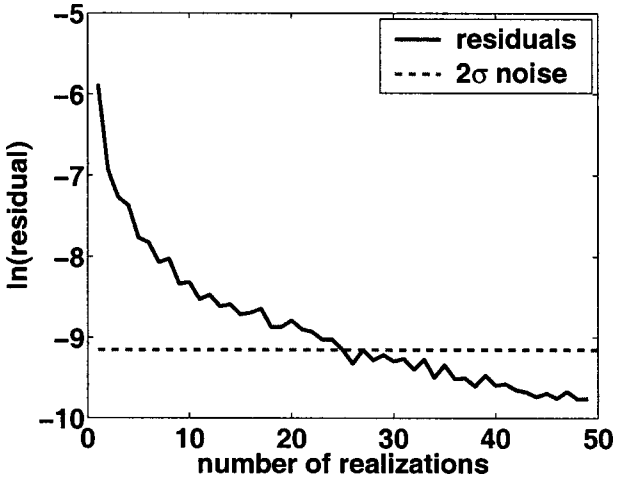

FIG. 4. Absolute value of the residual between the coherent wave field for n and $n-1$ realizations. The horizontal line is two standard deviations of the background noise level, as recorded before the arrival of the coherent wave.

B. Multiple scattering

On the face of the model with the disordered pattern of grooves, we record ensembles of ultrasonic wave fields at 43 source-detector distances, on a line perpendicular to the grooves. Figure 3 contains the ensemble for $x=4$ cm. The coherent intensity is the square of the average of the wave fields, whereas the total intensity is the average of the squared wave fields. The incoherent intensity is the total minus the coherent intensity. For $x \leqslant 52$ mm, each ensemble contains 50 realizations, but due to the limited size of the model, this number of realizations drops for $x>52$ mm. However, the coherent wave field converges to within two standard deviations of the background noise level after 25 realizations (Fig. 4). This background noise level is estimated from recordings before the first energy arrives at the detector.

Because we are able to separate both the data and the solution to RT into a coherent and incoherent part, we can treat the parameter-fitting problem for each separately. Theoretically it is possible to invert for (ℓ_s, ℓ_a) with only the diffuse energy [6,40], but at late times these parameters are

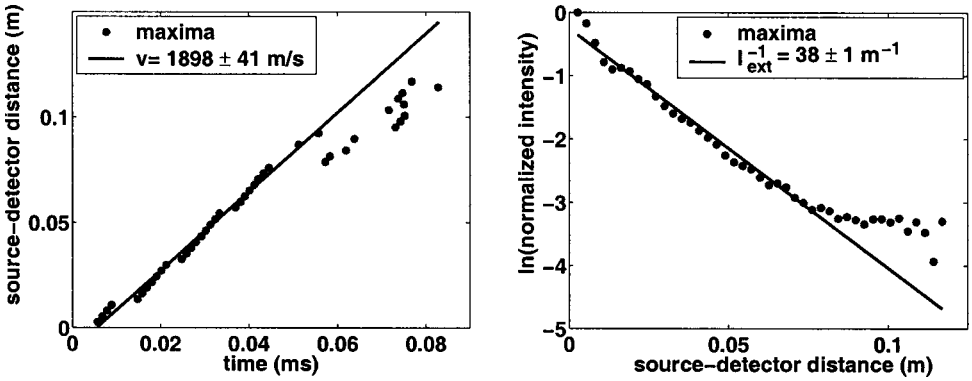

FIG. 5. Regressions for the energy velocity (left) and decay of the coherent intensity (right), for those source-detector distances where ensemble averaging has converged to within the background noise level.

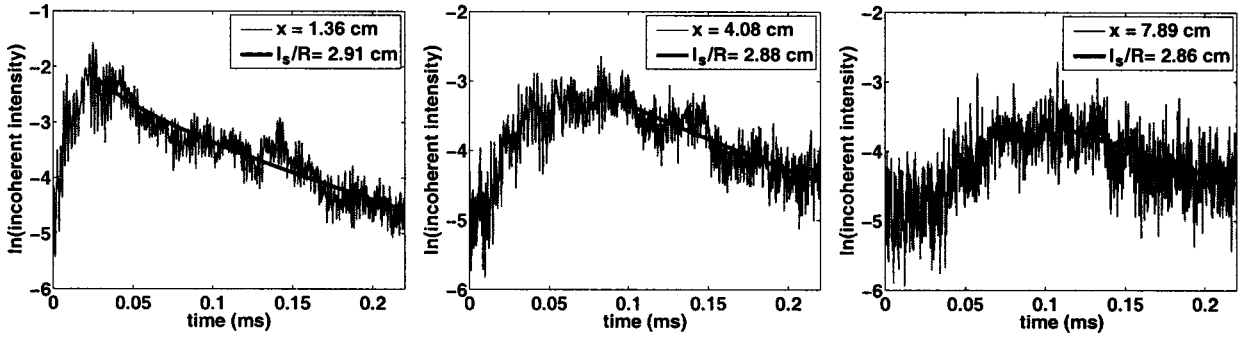

FIG. 6. Measured and modeled incoherent intensity for three of the 43 source-detector distances x. Each modeled signal is an independent best fit to the data in the least-squares sense.

coupled in the expression for the total intensity (Eqs. 14–23 of Ref. [2]).

The group velocity is estimated by a regression on the slope of the peak of the coherent intensity for those source-detector distances that have ample ensemble averaging, plotted in the left panel of Fig. 5. The resulting velocity is 1898 ± 41 m/s. In the absence of resonant scattering, this velocity is generally considered to be the energy velocity [23,41]. The right panel contains the regression on the natural logarithm of the decay of the coherent intensity, leading to $\ell_{\mathrm{ext}}=38\pm 1$ m.

The incoherent intensity is the thin line in Fig. 6. The thick lines are the best fits in the least-squares sense for the incoherent part of Eq. (2), using the average velocity and ℓ_{ext} as estimated from the coherent signal.

Estimates of R/ℓ_s for each of the 43 source-detector distances are plotted in Fig. 7, leading to $\ell_s/R=2.92\pm 0.08$ cm and $\ell_a=33\pm 17$ cm.

III. DISCUSSION

While theoretically in infinite 1D random media energy becomes localized, truly 1D models are difficult to achieve in practice: plane waves extending to infinity would have to be incident on perfectly planar layers, for example. In the literature, the distinction is made between the wave field in disordered chains, or a single string of particles, versus a wire [42]. Even though macroscopically 1D, at the microscopic level the wire can be treated as a number of chains connected by transverse channels. These channels reduce the interference effects necessary to bring the system into a localized state. In other words, localization occurs only when the Thouless energy is greater than the mean level spacing (e.g., [15,42]), even in 1D geometries such as wires or our surface wave model. We found that a 1D RT model explains energy propagation inside the scattering medium for distances up to several times R/ℓ_s (Fig. 7) and thus does not appear to be localized: [39] contains movies of a localized numerical simulation versus measured energy propagation in the groove sequence, supporting this observation. It is our belief that the microscopically complicated scattering process that we measured on a single groove provides enough paths for scattered waves to avoid the level of interference necessary to induce localization.

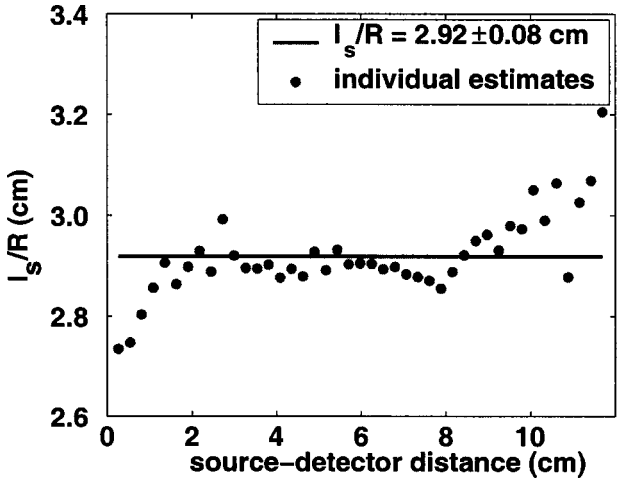

FIG. 7. Estimates of ℓ_s/R as a function of x. Individual estimates are from independent least-squares fits to the measured incoherent intensity as illustrated in Fig. 6.

Even though we can fit the data with an average $R/\ell_s=2.92$ cm, values for the smallest and largest source-detector distances deviate slightly from average. While the diffusion approximation seems to be accurate after a number of scattering mean free paths [16,43], we find that RT describes the energy propagation to within the noise level after $x\sim R/\ell_s$. For large x, deviations from the average R/ℓ_s can be attributed to a number of factors. First, for $x>75$ mm, size limitations on the block do not allow us to gather the 25 realizations necessary for the coherent intensity to converge. Secondly, the signal-to-noise ratio drops for larger propagation distances in the scattering sequence. Finally—as recording time is limited by the dimensions of the model—for larger source-detector distances, the least-squares fit to the incoherent signal is on a smaller time window, making the fit less accurate (see the right panel of Fig. 6).

As noted, in 1D, $1/\ell_{\mathrm{ext}}=R/\ell_s+1/\ell_a$. We estimate $R=0.15$ for a single groove from Fig. 1. However, because we have several grooves per wavelength in the multiple scattering case, the independent scattering approximation is likely violated, and R might differ. However, if $R=0.15$, then $\ell_s\approx 4$ mm. Because $1/\ell_{\mathrm{ext}}=1/\ell_s+1/\ell_a$ in dimensions >1, solutions to RT are often cast in terms of ℓ_s, which in our

casewould lead to misinterpretation of the data. Strictly speaking, a more general solution to RT should be formulated in terms of ℓ_{ext}.

IV. CONCLUSIONS

A 1D anisotropic radiative transfer model describes energy transport in a laboratory model of strong ultrasonic multiple scattering in the region around a scattering mean free path, suggesting the localization length is significantly greater than the scattering mean free path. Fitting both the coherent and incoherent energy allows us to resolve the scattering and absorption mean free path to greater accuracy than a late-time diffusion fit can provide.

ACKNOWLEDGMENTS

The authors thank Roel Snieder, Bart van Tiggelen, Ping Sheng, Azriel Genack, Ludovic Margerin and everyone in PAL for many helpful discussions. This work was supported by the Consortium Project on Seismic Inverse Methods for Complex Structures at the Center for Wave Phenomena, the National Science Foundation (EAR-0111804 and EAR-0337379), and the Army Research Office (DAAG55-98-1-0277 and DAAD19-03-1-0292).

[1] P. W. Anderson, Phys. Rev. **109**, 1492 (1958).
[2] A. Ishimaru, *Wave Propagation and Scattering in Random Media* (Oxford University Press, Oxford, 1997).
[3] P. Sheng, *Introduction to Wave Scattering, Localization and Mesoscopic Phenomena* (Academic Press, San Diego, 1995).
[4] J. L. Thomas, F. Wu, and M. Fink, Ultrason. Imaging **18**, 106 (1996).
[5] D. A. Boas, L. E. Campbell, and A. G. Yodh, Phys. Rev. Lett. **75**, 1855 (1995).
[6] L. Margerin, M. Campillo, N. M. Shapiro, and B. A. van Tiggelen, Geophys. J. Int. **138**, 343 (1999).
[7] R. F. O'Doherty and N. A. Anstey, Geophys. Prospect. **19**, 430 (1971).
[8] M. Haney, K. van Wijk, and R. K. Snieder, available at http://acoustics.mines.edu
[9] W. A. Kuperman, W. Hodgkiss, H. C. Song, T. Akal, C. Ferla, and D. R. Jackson, J. Acoust. Soc. Am. **102**, 1 (1997).
[10] A. Derode, A. Tourin, J. de Rosny, M. Tanter, S. Yon, and M. Fink, Phys. Rev. Lett. **90**, 014301 (2003).
[11] D. S. Wiersma, P. Bartolini, A. Lagendijk, and R. Righini, Nature (London) **390**, 671 (1997).
[12] F. Scheffold and G. Maret, Phys. Rev. Lett. **81**, 5800 (1998).
[13] M. Haney and R. K. Snieder, Phys. Rev. Lett. **91**, 093902 (2003).
[14] A. A. Chabanov, Z. Q. Zhang, and A. Z. Genack, Phys. Rev. Lett. **90**, 203903 (2003).
[15] B. A. van Tiggelen, in *Diffuse Waves in Complex Media*, Vol. 531 of *NATO Science Series C: Mathematical and Physical Sciences*, edited by J. P. Fouque (Kluwer, Boston, 1999), pp. 1–60.
[16] Z. Q. Zhang, I. P. Jones, H. P. Schriemer, J. H. P. D. A. Weitz, and P. Sheng, Phys. Rev. E **60**, 4843 (1999).
[17] A. Tourin, A. Derode, P. Roux, B. van Tiggelen, and M. Fink, Phys. Rev. Lett. **79**, 3637 (1997).
[18] A. Mirlin, Phys. Rep. **326**, 259 (2000).
[19] H. Moritz, T. Stöferle, M. Köhl, and T. Esslinger, Phys. Rev. Lett. **91**, 250402 (2003).
[20] F. M. Izrailev, J. A. Méndez-Bermúdez, and G. A. Luna-Acosta, Phys. Rev. E **68**, 066201 (2003).
[21] S. K. Gray and T. Kupka, Phys. Rev. B **68**, 045415 (2003).
[22] I. Zambetaki, Q. Li, E. N. Economou, and C. M. Soukolis, Phys. Rev. B **56**, 12 221 (1997).
[23] H. P. Schriemer, M. L. Cowan, J. H. Page, P. Sheng, Z. Liu, and D. A. Weitz, Phys. Rev. Lett. **79**, 3166 (1997).
[24] R. L. Weaver and W. Sachse, J. Acoust. Soc. Am. **97**, 2094 (1995).
[25] G. A. Cwillich, Nanotechnology **13**, 274 (2002).
[26] P. Carpena, V. Gasparian, and M. Ortuño, Phys. Rev. B **51**, 12813 (1995).
[27] L. Dal Negro, C. J. Oton, Z. Gaburro, L. Pavesi, P. Johnson, A. Lagendijk, R. Righini, M. Colocci, and D. S. Wiersma, Phys. Rev. Lett. **90**, 055501 (2003).
[28] J. A. Scales and K. van Wijk, Appl. Phys. Lett. **74**, 3899 (1999).
[29] J. A. Scales and K. van Wijk, Appl. Phys. Lett. **79**, 2294 (2001).
[30] K. van Wijk, Ph.D. thesis, Colorado School of Mines (2003).
[31] K. van Wijk, D. Komatitsch, J. A. Scales, and J. Tromp, J. Acoust. Soc. Am. **115**, 1006 (2004).
[32] P. Morse and H. Feshbach, *Methods of Theoretical Physics* (McGraw-Hill, New York, 1953).
[33] J. C. Paasschens, Phys. Rev. E **56**, 1135 (1997).
[34] P. A. Lemieux, M. U. Vera, and D. J. Durian, Phys. Rev. E **57**, 4498 (1998).
[35] G. H. Goedecke, J. Opt. Soc. Am. **67**, 1339 (1977).
[36] D. J. Durian and J. Rudnick, J. Opt. Soc. Am. A **14**, 235 (1996).
[37] P. C. Hemmer, Physica (Amsterdam) **27**, 79 (1961).
[38] I. A. D. Viktorov, *Rayleigh & Lamb Waves. Physical Theory and Application* (Plenum, New York, 1967).
[39] http://acoustics.mines.edu/onedee.html (2003).
[40] U. Wegler and B. Lühr, Geophys. J. Int. **145**, 579 (2001).
[41] M. P. van Albada, B. A. van Tiggelen, A. Lagendijk, and A. Tip, Phys. Rev. Lett. **66**, 3132 (1991).
[42] K. Efetov, *Supersymmetry in Disorder and Chaos* (Cambridge University Press, Cambridge, 1997).
[43] K. M. Yoo, Feng Liu, and R. R. Alfonso, Phys. Rev. Lett. **64**, 2647 (1990).
[44] W. Gellermann, M. Kohmoto, B. Sutherland, and P. C. Taylor, Phys. Rev. Lett. **72**, 633 (1994).
[45] Originally we chose a Fibonacci model in order to exploit analytic and experimental work on localization and band gaps (e.g., [44]). However, in practice even computer-numerically-controlled machining of the grooves resulted in small random variations, as revealed by high-resolution optical scans [31]. Numerical modeling shows that these small variations are visible in the multiple scattering coda. Hence, for this work the model is effectively random.